

## TFBSFootprinter: a multiomics tool for prediction of transcription factor binding sites in vertebrate species

Harlan R. Barker, Seppo Parkkila & Martti E. E. Tolvanen

To cite this article: Harlan R. Barker, Seppo Parkkila & Martti E. E. Tolvanen (2025) TFBSFootprinter: a multiomics tool for prediction of transcription factor binding sites in vertebrate species, *Transcription*, 16:2-3, 204-223, DOI: [10.1080/21541264.2025.2521764](https://doi.org/10.1080/21541264.2025.2521764)

To link to this article: <https://doi.org/10.1080/21541264.2025.2521764>



© 2025 The Author(s). Published by Informa UK Limited, trading as Taylor & Francis Group.



Published online: 11 Jul 2025.



Submit your article to this journal [↗](#)



Article views: 229



View related articles [↗](#)



View Crossmark data [↗](#)

# TFBSFootprinter: a multiomics tool for prediction of transcription factor binding sites in vertebrate species

Harlan R. Barker <sup>a,b,c</sup>, Seppo Parkkila<sup>a,b</sup>, and Martti E. Tolvanen<sup>d</sup>

<sup>a</sup>Tampere University Hospital and Faculty of Medicine and Health Technology, Tampere University, Tampere, Finland; <sup>b</sup>Department of Clinical Chemistry, Fimlab Laboratories PLC, Tampere University Hospital, Tampere, Finland; <sup>c</sup>Disease Networks Unit, Faculty of Biochemistry and Molecular Medicine, University of Oulu, Oulu, Finland; <sup>d</sup>Department of Computing, University of Turku, Turku, Finland

## ABSTRACT

**Background:** Transcription factor (TF) proteins play a critical role in the regulation of eukaryotic gene expression via sequence-specific binding to genomic locations known as transcription factor binding sites (TFBSs). Accurate prediction of TFBSs is essential for understanding gene regulation, disease mechanisms, and drug discovery. These studies are therefore relevant not only in humans but also in model organisms and domesticated and wild animals. However, current tools for the automatic analysis of TFBSs in gene promoter regions are limited in their usability across multiple species. To our knowledge, no tools currently exist that allow for automatic analysis of TFBSs in gene promoter regions for many species.

**Methodology and Findings:** The TFBSFootprinter tool combines multiomic transcription-relevant data for more accurate prediction of functional TFBSs in 317 vertebrate species. In humans, this includes vertebrate sequence conservation (GERP), proximity to transcription start sites (FANTOM5), correlation of expression between target genes and TFs predicted to bind promoters (FANTOM5), overlap with ChIP-Seq TF metaclusters (GTRD), overlap with ATAC-Seq peaks (ENCODE), eQTLs (GTEx), and the observed/expected CpG ratio (Ensembl). In non-human vertebrates, this includes GERP, proximity to transcription start sites, and CpG ratio.

TFBSFootprinter analyses are based on the Ensembl transcript ID for simplicity of use and require minimal setup steps. Benchmarking of the TFBSFootprinter on a manually curated and experimentally verified dataset of TFBSs produced superior results when using all multiomic data (average area under the receiver operating characteristic curve, 0.881), compared with DeepBind (0.798), DeepSEA (0.682), FIMO (0.817) and traditional PWM (0.854). The results were further improved by selecting the best overall combination of multiomic data (0.910). Additionally, we determined combinations of multiomic data that provide the best model of binding for each TF. TFBSFootprinter is available as Conda and Python packages.

## ARTICLE HISTORY

Received 14 January 2025

Revised 19 May 2025

Accepted 12 June 2025

## KEYWORDS



Transcription factor binding site; promoter; gene regulation; multiomics; vertebrate; bioinformatics

## Introduction

Transcription factor (TF) proteins play a critical role in the regulation of eukaryotic gene expression by sequence-specific binding to short stretches of DNA (6–24 bp) known as transcription factor binding sites (TFBSs) [1] which can comprise larger genomic locations known as cis-regulatory elements (CREs) [2]. Promoters and enhancers are the most common types of CREs and TF binding in these regions is ultimately responsible for activating, enhancing, and repressing gene expression programs [1,2]. Because of the role these proteins play in transcription, the discovery of TFBSs greatly furthers the

understanding of many, if not all, biological processes [1]. In previous works we have used TFBS prediction to derive insights about gene expression in studies of wound healing [3], brain tumors [4], and SARS-CoV-2 [5,6].

Many tools have been created to identify TFBSs. Depending on the approach, the extent of incorporation of relevant experimental data varies widely. Early on, the position weight matrix (PWM) was used to represent and predict the binding of proteins to DNA. The PWM can then be used to obtain a likelihood score for a target DNA region, which thus represents the likelihood of a TF binding to that DNA sequence.

**CONTACT** Harlan R. Barker  [Harlan.Barker@tuni.fi](mailto:Harlan.Barker@tuni.fi)  Tampere University Hospital and Faculty of Medicine and Health Technology, Tampere University, Arvo Ylpön Katu 34 F367, Tampere 33520, Finland

© 2025 The Author(s). Published by Informa UK Limited, trading as Taylor & Francis Group.

This is an Open Access article distributed under the terms of the Creative Commons Attribution License (<http://creativecommons.org/licenses/by/4.0/>), which permits unrestricted use, distribution, and reproduction in any medium, provided the original work is properly cited. The terms on which this article has been published allow the posting of the Accepted Manuscript in a repository by the author(s) or with their consent.

In the search for increased accuracy, newer models have improved TFBS prediction by incorporating other relevant biological data, such as 3D structure of DNA [7–11], chromatin accessibility/DNase hypersensitivity sites [12–14], overlap in gene ontology [15], amino acid physicochemical properties [16], and gene expression and chromatin accessibility [17,18]. These alternative models often match or outperform strictly sequence-based models [11,19] in the prediction of TFBSs, although they may involve inefficient and/or underdeveloped technologies compared with the more widely used ChIP-Seq and SELEX approaches. However, this varies by TF, and therefore, it may make sense to derive individual models composed of the most relevant contextual data for each [20]. In addition, algorithms for *ab initio* motif discovery and enrichment from *in vivo* data, such as HOMER [21], STEME [22], ProSampler [23], and STREME [24], which are reviewed here [25], are also under development. Correspondingly, several databases catalog TF motifs, most prominently JASPAR [26,27] and TRANSFAC [28].

### ***TFBSFootprinter incorporates multiomic transcription-relevant data***

We sought to identify multiple sources of experimental data relevant to gene expression and TF binding and to incorporate them into a comprehensive model to improve the prediction of functional TFBSs. Specifically, clustering of TFBSs has been shown to be an indicator of functionality [29–31]; conservation of genetic sequences across genomes of related species is one of the most successfully used attributes in the identification of TFBSs [31,32]; proximity to the transcription start site (TSS) is strongly linked to TFBS functionality [33]; correlation of expression between a TF and another gene is an indication of a functional relationship [17,34,35]; variants in noncoding regions have a demonstrated effect on gene expression [36–38]; and variants affecting gene expression are enriched in TFBSs [39]; open chromatin regions (ascertained by ATAC-Seq or DNase sensitivity) correlate with TF binding [40]; and finally, as previously mentioned, significant effort has gone

into identifying the actual composition of the binding sites themselves through the use of sequencing of TFBSs (e.g., ChIP-Seq and HT-SELEX) [41,42] as cataloged in several extensive databases, such as ReMap [43], the Cistrome Data Browser [44], and the Gene Transcription Regulation Database (GTRD) [45].

### ***Ensembl identifier-oriented system of analyses allows analyses in many species***

For our tool, the Ensembl transcript ID was chosen as the basic unit of reference. As a result, the tool we present here – TFBSFootprinter – can offer predictions in 317 vertebrates at the time of writing, including many model organisms and domesticated and wild animals (Table 1). From human and model organisms such as mouse and zebrafish to African bush elephant, the catalog can increase as the Ensembl database itself expands. Additionally, it allows the inclusion of important datasets that are gene-centric, such as FANTOM [46] TSSs and expression data, GTEx [36] expression quantitative trait loci (eQTLs), and all annotations that are compiled within Ensembl itself. Finally, the Ensembl transcript ID provides an easy point of reference for a greater audience of scientists, thus increasing the accessibility and utility of the tool.

## **Methods**

### ***Ensembl sequence retrieval***

The Ensembl Representational State Transfer (REST) server application programming interface (API) [47] is used by TFBSFootprinter for automated retrieval of user-defined DNA sequences near the transcription start site of an established Ensembl transcript ID. Annotations for the transcript and Ensembl-defined regulatory regions (e.g., “promoter flanking region”) are also retrieved and mapped in the final output figure.

### ***PWMs***

A total of 575 TF position frequency matrices (PFMs) retrieved from the JASPAR database [48]

**Table 1.** Ensembl species in which TFBSFootprinter analysis can be performed.

species name	species common name	species taxon	species assembly
<i>Acanthochromis polyacanthus</i>	spiny chromis	80966	ASM210954v1
<i>Accipiter nisus</i>	Eurasian sparrowhawk	211598	Accipiter nisus ver1.0
<i>Ailuropoda melanoleuca</i>	giant panda	9646	ASM200744v2
<i>Amazona collaria</i>	yellow-billed parrot	241587	ASM394721v1
<i>Amphilophus citrinellus</i>	Midas cichlid	61819	Midas v5
<i>Amphiprion ocellaris</i>	clown anemonefish	80972	ASM2253959v1
<i>Amphiprion percula</i>	orange clownfish	161767	Nemo v1
<i>Anabas testudineus</i>	climbing perch	64144	fAnaTes1.3
<i>Anas platyrhynchos</i>	mallard	8839	ASM874695v1
<i>Anas platyrhynchos platyrhynchos</i>	common mallard	8840	CAU duck1.0
<i>Anas zonorhyncha</i>	Eastern spot-billed duck	75864	ASM222487v1
<i>Anolis carolinensis</i>	green anole	28377	AnoCar2.0v2
<i>Anser brachyrhynchus</i>	pink-footed goose	132585	ASM259213v1
<i>Anser cygnoides</i>	swan goose	8845	GooseV1.0
<i>Aotus nancymae</i>	Ma's night monkey	37293	Anan 2.0
<i>Apteryx haastii</i>	Great spotted kiwi	8823	aptHaa1
<i>Apteryx owenii</i>	little spotted kiwi	8824	aptOwe1
<i>Apteryx rowi</i>	Okarito brown kiwi	308060	aptRow1
<i>Aquila chrysaetos chrysaetos</i>	golden eagle	223781	bAquChr1.2
<i>Astatotilapia calliptera</i>	eastern happy	8154	fAstCal1.3
<i>Astyanax mexicanus</i>	Mexican tetra	7994	Astyanax mexicanus-2.0
<i>Astyanax mexicanus pachon</i>	Pachon cavefish	7994	Astyanax mexicanus-1.0.2
<i>Athene cucularia</i>	burrowing owl	194338	athCun1
<i>Balaenoptera musculus</i>	Blue whale	9771	mBalMus1.v2
<i>Betta splendens</i>	Siamese fighting fish	158456	fBetSpl5.2
<i>Bison bison bison</i>	American bison	43346	Bison UMD1.0
<i>Bos grunniens</i>	domestic yak	30521	LU Bosgru v3.0
<i>Bos indicus hybrid</i>	hybrid cattle	30522	UOA Brahman 1
<i>Bos mutus</i>	wild yak	72004	BosGru v2.0
<i>Bos taurus</i>	cattle	9913	ARS-UCD1.3
<i>Bos taurus hybrid</i>	hybrid cattle	30522	UOA Angus 1
<i>Bubo bubo</i>	Eurasian eagle-owl	30461	BubBub1.0
<i>Buteo japonicus</i>	eastern buzzard	224669	ButJap1.0
<i>Caenorhabditis elegans</i>	<i>C.elegans</i>	6239	WBcel235
<i>Cairina moschata domestica</i>	muscovy Duck (domestic type)	1240228	CaiMos1.0
<i>Calidris pugnax</i>	ruff	198806	ASM143184v1
<i>Calidris pygmaea</i>	Spoon-billed sandpiper	425635	ASM369795v1
<i>Callithrix jacchus</i>	white-tufted-ear marmoset	9483	mCalJac1.pat.X
<i>Callorhynchus milii</i>	elephant shark	7868	Callorhynchus milii-6.1.3
<i>Camarhynchus parvulus</i>	small tree finch	87175	Camarhynchus parvulus V1.1
<i>Camelus dromedarius</i>	Arabian camel	9838	CamDro2
<i>Canis lupus dingo</i>	dingo	286419	ASM325472v1
<i>Canis lupus familiaris</i>	dog	9615	ROS Cfam 1.0
<i>Canis lupus familiarisbasenji</i>	dog	9615	Basenji breed-1.1
<i>Canis lupus familiarisboxer</i>	dog	9615	Dog10K Boxer Tasha
<i>Canis lupus familiarisgreatdane</i>	dog	9615	UMICH Zoey 3.1
<i>Canis lupus familiarisgsd</i>	dog	9615	UU Cfam GSD 1.0
<i>Capra hircus</i>	Goat	9925	ARS1
<i>Capra hircus blackbengal</i>	Goat	9925	CVASU BBG 1.0
<i>Carassius auratus</i>	goldfish	7957	ASM336829v1
<i>Carlito syrichta</i>	Philippine tarsier	1868482	Tarsius syrichta-2.0.1
<i>Castor canadensis</i>	American beaver	51338	C.can genome v1.0
<i>Catagonus wagneri</i>	Chacoan peccary	51154	CatWag v2 BIUU UCD
<i>Catharus ustulatus</i>	Swainson's thrush	91951	bCatUst1.pri
<i>Cavia aperea</i>	Brazilian guinea pig	37548	CavAp1.0
<i>Cavia porcellus</i>	domestic guinea pig	10141	Cavpor3.0
<i>Cebus imitator</i>	Panamanian white-faced capuchin	2715852	Cebus imitator-1.0
<i>Cercocebus atys</i>	Sooty mangabey	9531	Caty 1.0
<i>Cervus hanglu yarkandensis</i>	Yarkand deer	84702	CEY v1
<i>Chelonoidis abingdonii</i>	Abingdon island giant tortoise	106734	ASM359739v1
<i>Chelydra serpentina</i>	Common snapping turtle	8475	Chelydra serpentina-1.0
<i>Chinchilla lanigera</i>	Long-tailed chinchilla	34839	ChiLan1.0
<i>Chlorocebus sabaeus</i>	African green monkey	60711	ChISab1.1
<i>Choloepus hoffmanni</i>	Hoffmann's two-fingered sloth	9358	choHof1

(Continued)

Table 1. (Continued).

species name	species common name	species taxon	species assembly
<i>Chrysemys picta bellii</i>	Western painted turtle	8478	Chrysemys picta bellii-3.0.3
<i>Chrysolophus pictus</i>	golden pheasant	9089	Chrysolophus pictus GenomeV1.0
<i>Ciona intestinalis</i>	Sea squirt <i>Ciona intestinalis</i>	7719	KH
<i>Ciona savignyi</i>	Sea squirt <i>Ciona savignyi</i>	51511	CSAV2.0
<i>Clupea harengus</i>	Atlantic herring	7950	Ch v2.0.2v2
<i>Colobus angolensis palliatus</i>	Angola colobus	336983	Cang.pa 1.0
<i>Corvus moneduloides</i>	New Caledonian crow	1196302	bCorMon1.pri
<i>Cottoperca gobio</i>	channel bull blenny	56716	fCotGob3.1
<i>Coturnix japonica</i>	Japanese quail	93934	Coturnix japonica 2.0
<i>Cricetulus griseus chok1gshd</i>	Chinese hamster	10029	CHOK1GS HDv1
<i>Cricetulus griseus crigri</i>	Chinese hamster	10029	CriGri 1.0
<i>Cricetulus griseus picr</i>	Chinese hamster	10029	CriGri-PICRH-1.0
<i>Crocodylus porosus</i>	Australian saltwater crocodile	8502	CroPor comp1
<i>Cyanistes caeruleus</i>	blue tit	156563	cyaCae2
<i>Cyclopterus lumpus</i>	lumpfish	8103	fCycLum1.pri
<i>Cynoglossus semilaevis</i>	tongue sole	244447	Cse v1.0
<i>Cyprinodon variegatus</i>	sheepshead minnow	28743	C variegatus-1.0
<i>Cyprinus carpio carpio</i>	common carp	630221	Cypcar WagV4.0
<i>Cyprinus carpio germanmirror</i>	common carp german mirror	7962	German Mirror carp 1.0
<i>Cyprinus carpio hebaored</i>	common carp hebaored	7962	Hebaored carp 1.0
<i>Cyprinus carpio huanghe</i>	common carp huanghe	7962	Hunaghe carp 2.0
<i>Danio rerio</i>	zebrafish	7955	GRCz11
<i>Dasypus novemcinctus</i>	nine-banded armadillo	9361	Dasnov3.0
<i>Delphinapterus leucas</i>	beluga whale	9749	ASM228892v3
<i>Denticeps clupeioides</i>	denticle herring	299321	fDenClu1.2
<i>Dicentrarchus labrax</i>	European seabass	13489	dlabrax2021
<i>Dipodomys ordii</i>	Ord's kangaroo rat	10020	Dord 2.0
<i>Dromaius novaehollandiae</i>	emu	8790	droNov1
<i>Drosophila melanogaster</i>	Fruit fly	7227	BDGP6.46
<i>Echeneis naucrates</i>	live sharksucker	173247	fEcheNa1.1
<i>Echinops telfairi</i>	small Madagascar hedgehog	9371	TENREC
<i>Electrophorus electricus</i>	electric eel	8005	fEleEle1.pri
<i>Eptatretus burgeri</i>	Inshore hagfish	7764	Eburgeri 3.2
<i>Equus asinus</i>	ass	9793	ASM1607732v2
<i>Equus caballus</i>	horse	9796	EquCab3.0
<i>Erinaceus europaeus</i>	western European hedgehog	9365	HEDGEHOG
<i>Erpetoichthys calabaricus</i>	reedfish	27687	fErpCal1.1
<i>Erythrura gouldiae</i>	Gouldian finch	44316	GouldianFinch
<i>Esox lucius</i>	northern pike	8010	fEsoLuc1.pri
<i>Falco tinnunculus</i>	common kestrel	100819	FalTin1.0
<i>Felis catus</i>	domestic cat	9685	Felis catus 9.0
<i>Ficedula albicollis</i>	Collared flycatcher	59894	FicAlb1.5
<i>Fukomys damarensis</i>	Damara mole rat	885580	DMR v1.0
<i>Fundulus heteroclitus</i>	mummichog	8078	Fundulus heteroclitus-3.0.2
<i>Gadus morhua</i>	Atlantic cod	8049	gadMor3.0
<i>Gallus gallus</i>	chicken	9031	bGalGal1.mat.broiler.GRCg7b
<i>Gallus gallus gca000002315v5</i>	chicken	9031	GRCg6a
<i>Gallus gallus gca016700215v2</i>	chicken	9031	bGalGal1.pat.whiteleghornlayer.GRCg7w
<i>Gambusia affinis</i>	western mosquitofish	33528	ASM309773v1
<i>Gasterosteus aculeatus</i>	three-spined stickleback	481459	GAculeatus UGA version5
<i>Geospiza fortis</i>	medium ground-finch	48883	GeoFor 1.0
<i>Gopherus agassizii</i>	Agassiz's desert tortoise	38772	ASM289641v1
<i>Gopherus evgoodei</i>	Goodes thornscrub tortoise	1825980	rGopEvg1 v1.p
<i>Gorilla gorilla</i>	Western Lowland Gorilla	9595	gorGor4
<i>Gouania willdenowi</i>	blunt-snouted clingfish	441366	fGouWil2.1
<i>Haplochromis burtoni</i>	Burton's mouthbrooder	8153	AstBur1.0
<i>Heterocephalus glaber female</i>	naked mole-rat	10181	Naked mole-rat maternal
<i>Heterocephalus glaber male</i>	naked mole-rat	10181	Naked mole-rat paternal
<i>Hippocampus comes</i>	tiger tail seahorse	109280	H comes QL1 v1
<i>Homo sapiens</i>	Human	9606	GRCh38
<i>Hucho hucho</i>	huchen	62062	ASM331708v1
<i>Ictalurus punctatus</i>	channel catfish	7998	ASM400665v3
<i>Ictidomys tridecemlineatus</i>	thirteen-lined ground squirrel	43179	SpeTri2.0

(Continued)

Table 1. (Continued).

species name	species common name	species taxon	species assembly
Jaculus jaculus	Lesser Egyptian jerboa	51337	JacJac1.0
Junco hyemalis	dark-eyed junco	40217	ASM382977v1
Kryptolebias marmoratus	mangrove rivulus	37003	ASM164957v1
Labrus bergylta	ballan wrasse	56723	BallGen V1
Larimichthys crocea	large yellow croaker	215358	L crocea 2.0
Lates calcarifer	barramundi perch	8187	ASB HGAPassembly v1
Laticauda laticaudata	blue-ringed sea krait	8630	latLat 1.0
Latimeria chalumnae	coelacanth	7897	LatCha1
Lepidothrix coronata	blue-crowned manakin	321398	Lepidothrix coronata-1.0
Lepisosteus oculatus	Spotted gar	7918	LepOcu1
Leptobranchium leishanense	Leishan spiny toad	445787	ASM966780v1
Lonchura striata domestica	Bengalese finch	299123	LonStrDom1
Loxodonta africana	African savanna elephant	9785	loxAfr3
Lynx canadensis	Canada lynx	61383	mLynCan4 v1.p
Macaca fascicularis	Crab-eating macaque	9541	Macaca fascicularis 6.0
Macaca mulatta	Macaque	9544	Mmul 10
Macaca nemestrina	Pig-tailed macaque	9545	Mnem 1.0
Malurus cyaneus samueli	superb fairywren	2593467	mCya 1.0
Manacus vitellinus	golden-collared manakin	328815	ASM171598v2
Mandrillus leucophaeus	Drill	9568	Mleu.le 1.0
Marmota marmota marmota	Alpine marmot	9994	marMar2.1
Mastacembelus armatus	zig-zag eel	205130	fMasArm1.2
Maylandia zebra	zebra mbuna	106582	M zebra UMD2a
Meleagris gallopavo	turkey	9103	Turkey 5.1
Melopsittacus undulatus	budgerigar	13146	bMelUnd1.mat.Z
Meriones unguiculatus	Mongolian gerbil	10047	MunDraft-v1.0
Mesocricetus auratus	Golden Hamster	10036	MesAur1.0
Microcebus murinus	gray mouse lemur	30608	Mmur 3.0
Microtus ochrogaster	vole	79684	MicOch1.0
Mola mola	ocean sunfish	94237	ASM169857v1
Monodelphis domestica	gray short-tailed opossum	13616	ASM229v1
Monodon monoceros	narwhal	40151	NGI Narwhal 1
Monopterus albus	swamp eel	43700	M albus 1.0
Moschus moschiferus	Siberian musk deer	68415	MosMos v2 BIUU UCD
Mus caroli	Ryukyu mouse	10089	CAROLI EIJ v1.1
Mus musculus	mouse	10090	GRCm39
Mus musculus 129s1svimj	mouse	10090	129S1 SvImJ v1
Mus musculus aj	mouse	10090	A J v1
Mus musculus akrj	mouse	10090	AKR J v1
Mus musculus balbcj	mouse	10090	BALB cJ v1
Mus musculus c3hhej	mouse	10090	C3H HeJ v1
Mus musculus c57bl6nj	mouse	10090	C57BL 6NJ v1
Mus musculus casteij	mouse	10091	CAST Eij v1
Mus musculus cbaj	mouse	10090	CBA J v1
Mus musculus dba2j	mouse	10090	DBA 2J v1
Mus musculus fvbnej	mouse	10090	FVB NJ v1
Mus musculus lpj	mouse	10090	LP J v1
Mus musculus nodshiltj	mouse	10090	NOD SHiLtJ v1
Mus musculus nzohiltj	mouse	10090	NZO HILTJ v1
Mus musculus pwkphj	mouse	39442	PWK PhJ v1
Mus musculus wsbeij	mouse	10092	WSB Eij v1
Mus pahari	Shrew mouse	10093	PAHARI EIJ v1.1
Mus spicilegus	steppe mouse	10103	MUSP714
Mus spretus	algerian mouse	10096	SPRET Eij v1
Mustela putorius furo	Domestic ferret	9669	MusPutFur1.0
Myotis lucifugus	little brown bat	59463	Myoluc2.0
Myripristis murdjan	pinecone soldierfish	586833	fMyrMur1.1
Naja naja	Indian cobra	35670	Nana v5
Nannospalax galili	Upper Galilee mountains blind mole rat	1026970	S.galili v1.0
Neogobius melanostomus	round goby	47308	RGoby Basel V2
Neolamprologus brichardi	lyretail cichlid	32507	NeoBri1.0
Neovison vison	American mink	452646	NNQGG.v01
Nomascus leucogenys	Northern white-cheeked gibbon	61853	Nleu 3.0

(Continued)

Table 1. (Continued).

species name	species common name	species taxon	species assembly
<i>Notamacropus eugenii</i>	tammar wallaby	9315	Meug 1.0
<i>Notechis scutatus</i>	mainland tiger snake	8663	TS10Xv2-PRI
<i>Nothobranchius furzeri</i>	turquoise killifish	105023	Nfu 20,140,520
<i>Nothoprocta perdicaria</i>	Chilean tinamou	30464	notPer1
<i>Numida meleagris</i>	helmeted guineafowl	8996	NumMel1.0
<i>Ochotona princeps</i>	American pika	9978	OchPri2.0-Ens
<i>Octodon degus</i>	Degu	10160	OctDeg1.0
<i>Oncorhynchus kisutch</i>	coho salmon	8019	Okis V2
<i>Oncorhynchus mykiss</i>	rainbow trout	8022	USDA Omyka 1.1
<i>Oncorhynchus tshawytscha</i>	Chinook salmon	74940	Otsh v2.0
<i>Oreochromis aureus</i>	blue tilapia	47969	ZZ aureus
<i>Oreochromis niloticus</i>	Nile tilapia	8128	O niloticus UMD NMBU
<i>Ornithorhynchus anatinus</i>	platypus	9258	mOrnAna1.p.v1
<i>Oryctolagus cuniculus</i>	rabbit	9986	OryCun2.0
<i>Oryzias javanicus</i>	javanese ricefish	123683	OJAV 1.1
<i>Oryzias latipes</i>	Japanese medaka HdrR	8090	ASM223467v1
<i>Oryzias latipes hni</i>	Japanese medaka HNI	8090	ASM223471v1
<i>Oryzias latipes hsok</i>	Japanese medaka HSOK	8090	ASM223469v1
<i>Oryzias melastigma</i>	Indian medaka	30732	Om v0.7.RACA
<i>Oryzias sinensis</i>	Chinese medaka	183150	ASM858656v1
<i>Otolemur garnettii</i>	small-eared galago	30611	OtoGar3
<i>Otus sunia</i>	Oriental scops-owl	257818	OtuSun1.0
<i>Ovis aries</i>	sheep	9940	ARS-UI Ramb v2.0
<i>Ovis aries rambouillet</i>	sheep	9940	ARS-UI Ramb v2.0
<i>Pan paniscus</i>	bonobo	9597	panpan1.1
<i>Pan troglodytes</i>	chimpanzee	9598	Pan tro 3.0
<i>Panthera leo</i>	lion	9689	PanLeo1.0
<i>Panthera pardus</i>	leopard	9691	PanPar1.0
<i>Panthera tigris altaica</i>	Tiger	74533	PanTig1.0
<i>Papio anubis</i>	olive baboon	9555	Panubis1.0
<i>Parambassis ranga</i>	Indian glassy fish	210632	fParRan2.2
<i>Paramormyrops kingsleyae</i>	Paramormyrops kingsleyae	1676925	PKINGS 0.1
<i>Parus major</i>	Great Tit	9157	Parus major1.1
<i>Pavo cristatus</i>	Indian peafowl	9049	AIIM Pcri 1.0
<i>Pelodiscus sinensis</i>	Chinese softshell turtle	13735	PelSin 1.0
<i>Pelusios castaneus</i>	West African mud turtle	367368	Pelusios castaneus-1.0
<i>Periophthalmus magnuspinnatus</i>	<i>Periophthalmus magnuspinnatus</i>	409849	PM.fa
<i>Promyscus maniculatus bairdii</i>	Northern American deer mouse	230844	HU Pman 2.1
<i>Petromyzon marinus</i>	sea lamprey	7757	Pmarinus 7.0
<i>Phascolarctos cinereus</i>	koala	38626	phaCin unsw v4.1
<i>Phasianus colchicus</i>	Ring-necked pheasant	9054	ASM414374v1
<i>Phocoena sinus</i>	vaquita	42100	mPhoSin1.pri
<i>Physeter catodon</i>	sperm whale	9755	ASM283717v2
<i>Piliocolobus tephrosceles</i>	Ugandan red Colobus	591936	ASM277652v2
<i>Podarcis muralis</i>	common wall lizard	64176	PodMur 1.0
<i>Poecilia formosa</i>	Amazon molly	48698	PoeFor 5.1.2
<i>Poecilia latipinna</i>	sailfin molly	48699	P latipinna-1.0
<i>Poecilia mexicana</i>	shortfin molly	48701	P mexicana-1.0
<i>Poecilia reticulata</i>	guppy	8081	Guppy female 1.0 MT
<i>Pogona vitticeps</i>	central bearded dragon	103695	pvi1.1
<i>Pongo abelii</i>	Sumatran orangutan	9601	Susie PABv2
<i>Procavia capensis</i>	cape rock hyrax	9813	proCap1
<i>Prolemur simus</i>	greater bamboo lemur	1328070	Prosim 1.0
<i>Propithecus coquereli</i>	Coquerel's sifaka	379532	Pcoq 1.0
<i>Pseudonaja textilis</i>	eastern brown snake	8673	EBS10Xv2-PRI
<i>Pteropus vampyrus</i>	large flying fox	132908	pteVam1
<i>Pundamilia nyererei</i>	Makobe Island cichlid	303518	PunNye1.0
<i>Pygocentrus nattereri</i>	red-bellied piranha	42514	fPygNat1.pri
<i>Rattus norvegicus</i>	Norway rat	10116	mRatBN7.2
<i>Rattus norvegicus shrspbbbutx</i>	Norway rat	10116	UTH Rnor SHRSP BbbUtx 1.0
<i>Rattus norvegicus shrutx</i>	Norway rat	10116	UTH Rnor SHR Utx
<i>Rattus norvegicus wkybbb</i>	Norway rat	10116	UTH Rnor WKY Bbb 1.0
<i>Rhinolophus ferrumequinum</i>	greater horseshoe bat	59479	mRhiFer1 v1.p

(Continued)

Table 1. (Continued).

species name	species common name	species taxon	species assembly
<i>Rhinopithecus bieti</i>	Black snub-nosed monkey	61621	ASM169854v1
<i>Rhinopithecus roxellana</i>	Golden snub-nosed monkey	61622	Rrox v1
<i>Saccharomyces cerevisiae</i>	baker's yeast	559292	R64-1-1
<i>Saimiri boliviensis boliviensis</i>	Bolivian squirrel monkey	39432	SaiBol1.0
<i>Salarias fasciatus</i>	jewelled blenny	181472	fSalaFa1.1
<i>Salmo salar</i>	Atlantic salmon	8030	Ssal v3.1
<i>Salmo trutta</i>	brown trout	8032	fSalTru1.1
<i>Salvator merianae</i>	Argentine black and white tegu	96440	HLtupMer3
<i>Sander lucioperca</i>	pike-perch	283035	SLUC FBN 1
<i>Sarcophilus harrisii</i>	Tasmanian devil	9305	mSarHar1.11
<i>Sciurus vulgaris</i>	Eurasian red squirrel	55149	mSciVul1.1
<i>Scleropages formosus</i>	Asian bonytongue	113540	fSclFor1.1
<i>Scophthalmus maximus</i>	turbot	52904	ASM1334776v1
<i>Serinus canaria</i>	common canary	9135	SCA1
<i>Seriola dumerili</i>	greater amberjack	41447	Sdu 1.0
<i>Seriola lalandi dorsalis</i>	yellowtail amberjack	1841481	Sedor1
<i>Sinocyclocheilus anshuiensis</i>	blind barbel	1608454	SAMN03320099.WGS v1.1
<i>Sinocyclocheilus grahami</i>	golden-line barbel	75366	SAMN03320097.WGS v1.1
<i>Sinocyclocheilus rhinoceros</i>	horned golden-line barbel	307959	SAMN03320098 v1.1
<i>Sorex araneus</i>	European shrew	42254	COMMON SHREW1
<i>Sparus aurata</i>	gilthead seabream	8175	fSpaAur1.1
<i>Spermophilus dauricus</i>	Daurian ground squirrel	99837	ASM240643v1
<i>Sphaeramia orbicularis</i>	orbiculate cardinalfish	375764	fSphaOr1.1
<i>Sphenodon punctatus</i>	tuatara	8508	ASM311381v1
<i>Stachyris ruficeps</i>	rufous-capped babbler	181631	ASM869450v1
<i>Stegastes partitus</i>	bicolor damselfish	144197	Stegastes partitus-1.0.2
<i>Strigops habroptila</i>	Kakapo	2489341	bStrHab1 v1.p
<i>Strix occidentalis caurina</i>	northern spotted owl	311401	Soccid v01
<i>Struthio camelus australis</i>	African ostrich	441894	ASM69896v1
<i>Suricata suricatta</i>	meerkat	37032	meerkat 22Aug2017 6uvM2 HiC
<i>Sus scrofa</i>	pig	9823	Sscrofa11.1
<i>Sus scrofa bamei</i>	pig	9823	Bamei pig v1
<i>Sus scrofa berkshire</i>	pig	9823	Berkshire pig v1
<i>Sus scrofa hampshire</i>	pig	9823	Hampshire pig v1
<i>Sus scrofa jinhua</i>	pig	9823	Jinhua pig v1
<i>Sus scrofa landrace</i>	pig	9823	Landrace pig v1
<i>Sus scrofa largewhite</i>	pig	9823	Large White v1
<i>Sus scrofa meishan</i>	pig	9823	Meishan pig v1
<i>Sus scrofa pietrain</i>	pig	9823	Pietrain pig v1
<i>Sus scrofa rongchang</i>	pig	9823	Rongchang pig v1
<i>Sus scrofa tibetan</i>	pig	9823	Tibetan Pig v2
<i>Sus scrofa usmarc</i>	pig	9823	USMARCv1.0
<i>Sus scrofa wuzhishan</i>	pig	9823	minipig v1.0
<i>Taeniopygia guttata</i>	zebra finch	59729	bTaeGut1 v1.p
<i>Takifugu rubripes</i>	fugu	31033	fTakRub1.2
<i>Terrapene carolina triunguis</i>	Three-toed box turtle	2587831	T m triunguis-2.0
<i>Tetraodon nigroviridis</i>	spotted green pufferfish	99883	TETRAODON8
<i>Theropithecus gelada</i>	gelada	9565	Tgel 1.0
<i>Tupaia belangeri</i>	northern tree shrew	37347	TREESHREW
<i>Tursiops truncatus</i>	bottlenosed dolphin	9739	turTru1
<i>Urocitellus parryii</i>	Arctic ground squirrel	9999	ASM342692v1
<i>Ursus americanus</i>	American black bear	9643	ASM334442v1
<i>Ursus maritimus</i>	Polar bear	29073	UrsMar 1.0
<i>Ursus thibetanus thibetanus</i>	Asiatic black bear	441215	ASM966005v1
<i>Varanus komodoensis</i>	Komodo dragon	61221	ASM479886v1
<i>Vicugna pacos</i>	alpaca	30538	vicPac1
<i>Vombatus ursinus</i>	common wombat	29139	bare-nosed wombat genome assembly
<i>Vulpes vulpes</i>	red fox	9627	VulVul2.2
<i>Xenopus tropicalis</i>	tropical clawed frog	8364	UCB Xtro 10.0
<i>Xiphophorus couchianus</i>	Monterrey platyfish	32473	Xiphophorus couchianus-4.0.1
<i>Xiphophorus maculatus</i>	southern platyfish	8083	X maculatus-5.0-male
<i>Zalophus californianus</i>	california sea lion	9704	mZalCal1.pri
<i>Zonotrichia albicollis</i>	white-throated sparrow	44394	Zonotrichia albicollis-1.0.1
<i>Zosterops lateralis melanops</i>	silver-eye	1220523	ASM128173v1

(<http://jaspar.genereg.net/>; nonredundant) are used to create PWMs (Eq. 1), as described by [49]:

$$LLS_{\text{binding}} = \sum_{i=1}^N \log_2 \left( \frac{\frac{a_i + \frac{b}{4}}{S + b}}{\frac{n_{\text{nuc}} + b}{l_{\text{bg}} + b}} \right) \quad (1)$$

$N$  is the set of nucleotides in the currently scanned sequence;  $a_i$  is the number of instances of nucleotide  $a$  at position  $i$ ;  $b$  is a pseudocount set to 0.8 per [49];  $S$  is the number of sequences describing the motif;  $n_{\text{nuc}}$  is the count of the nucleotide in the background sequence; and  $l_{\text{bg}}$  is the length of the background sequence. The background frequencies for each nucleotide were set to match those of the human genome as determined previously [50].

### CAGE peak locations and Spearman correlation of expression values

Cap analysis of gene expression (CAGE) uses sequencing of cDNA generated from RNA to both determine TSSs and quantify their expression levels. The FANTOM project has performed CAGE across the human genome [46], and the results are freely available for download (<http://fantom.gsc.riken.jp/data/>). For non-human species “CAGE-like” peaks were derived using Ensembl RNA-Seq data for each of 218 species, as follows: 1) for each of 218 species, RNA-Seq data as BigWig files were downloaded ([ensembl.org/pub/release-113/data\\_files/{species\\_name}](http://ensembl.org/pub/release-113/data_files/{species_name})), in most cases a single merged file was available but if not all available files were merged using Bedtools (version 2.31.1); 2) all subsequent peaks were filtered by width of >10 nt and signal strength >5 and merged if within 10 nt of one another; 3) genome annotations were downloaded as GTF files ([ensembl.org/pub/release-113/gtf/{species\\_name}](http://ensembl.org/pub/release-113/gtf/{species_name})), and peaks occurring within 50 nt of an annotated TSS were associated to gene transcripts, and are described as “CAGE-like” peaks. Using the genomic locations of the FANTOM CAGE peaks or CAGE-like peaks (non-human species), the distances from each nucleotide position in the human genome to the nearest CAGE peak were calculated. The distribution of these distances was used to generate a log-likelihood score for all observed distances. The CAGE peak locations and distance/log-likelihood

score pairings are then used during de novo prediction of TFBSs (Eq. 2).

$$LLS_{\text{CAGE distances}} = \sum_{i=1}^N -\log_2 \left( P(x \leq d_i | \text{genome}) \cdot \frac{p_i}{P_{\text{total}}} \right) \quad (2)$$

Where  $N$  is the number of all CAGE peaks associated with the target gene;  $d_i$  is the distance to the current CAGE peak;  $p_i$  is the number of peak counts of the current CAGE peak; and  $p_{\text{total}}$  is the total peak count for this gene.

The expression data for CAGE peaks associated with the 575 JASPAR TF genes were then combined with the expression data for all CAGE peaks to perform a total of 386,652,770 Spearman correlation analyses via the “spearmanr” function from the SciPy Stats module [51]. Bonferroni correction was performed to account for multiple testing. Owing to the size of the analysis, a cutoff correlation magnitude value of 0.3 was used, and all the lower values ( $-0.3 < 0.3$ ) and correlation pairs were discarded. A distribution was generated from the resulting correlation data, which were used to generate log-likelihood scores for each possible correlation value (Eq. 3). The CAGE peak expression correlations/log-likelihood score pairings are then used during de novo prediction of TFBSs. Computation was performed via the supercomputing resources of the CSC – IT Center for Science Ltd.

$$LLS_{\text{expression correlation}} = -\log_2 P(x \geq c_{\text{current}} | c_{\text{all}}) \quad (3)$$

Where  $c_{\text{current}}$  is the Spearman correlation between the expression of the target gene and the expression of the TF corresponding to the putative TFBS and where  $c_{\text{all}}$  is the distribution of all Spearman correlations between JASPAR TF genes and all genes.

### Experimental TFBSs compiled by the GTRD

The GTRD project ([gtrd.biouml.org](http://gtrd.biouml.org)) is the largest comprehensive collection of uniformly processed human and mouse ChIP-Seq peaks and has compiled data from 8,828 experiments extracted from the Gene Expression Omnibus (GEO), Sequence Read Archive (SRA), and Encyclopedia of DNA Elements (ENCODE) databases [45]. One of the

outputs of the performed analyses is reads that have been grouped to identify “metaclusters”, places where TF binding events cluster together in the human genome. We retrieved the metacluster data (28,524,954 peaks) from the GTRD database (version 18.0) [52] and subsequently mapped the number of overlapping metaclusters for each nucleotide position in the human genome. The distribution of these overlaps was used to generate a log-likelihood score for all observed overlap counts. The metacluster locations and distance/log-likelihood score pairings are then used during de novo prediction of TFBSs (Eq. 4).

$$LLS_{\text{metaclusters}} = -\log_2 P(x \geq n_{\text{overlap}} | \text{human genome}) \quad (4)$$

Where  $n_{\text{overlap}}$  is the number of metaclusters overlapped by the current putative TFBS and where the  $D_{\text{human genome}}$  is the distribution of the number of overlapping metaclusters for every nucleotide position in the human genome.

### ATAC-Seq peaks

The assay for transposase-accessible chromatin using sequencing (ATAC-Seq) is an experimental method for revealing the location of open chromatin [53]. These locations are indicative of genomic regions that, owing to their unpacked nature, may allow TFs to bind to DNA and subsequently influence transcription. Open chromatin regions have been shown to be useful in the prediction of TFBSs [54]. We retrieved and compiled data from 135 ATAC-Seq experiments stored in the ENCODE project database ([www.encodeproject.org](http://www.encodeproject.org)) and mapped the distance from each nucleotide position in the human genome to the nearest ATAC-Seq peak, and the distribution of these distances was used to generate a log-likelihood score for all observed distances. The ATAC-Seq peak locations and distance/log-likelihood score pairings are then used during de novo prediction of TFBSs (Eq. 5).

$$LLS_{\text{ATAC-Seq distances}} = \sum_{i=0}^N -\log_2 P(x \leq d_i | \text{human genome}) \quad (5)$$

Where  $N$  is the number of ATAC-Seq peaks within the current target region;  $d_i$  is the distance

to the current ATAC-Seq peak; and  $D_{\text{human genome}}$  is the distribution of the distances to the nearest ATAC-Seq peak for each nucleotide position in the human genome.

### eQTLs

The genome tissue expression (GTEx) project ([gtexportal.org](http://gtexportal.org); version 7) has performed expression quantitative trait loci (eQTL) analysis on 10,294 samples from 48 tissues from 620 persons [36,55]. This analysis identified 7,621,511 variant locations in the genome, usually 1–5 base pairs (bp), that affect gene expression. eQTL data were extracted from the GTEx database and used to construct a distribution of the magnitude of effect on gene expression, which was then used to generate log-likelihood scores (Eq. 6). Next, we generated a second distribution of the distance from each gene to its variants; the distance was limited to 1,000,000 bp from either end of the transcript, as this is the search area over which GTEx scans for variants affecting the expression of each gene. The variant locations, magnitude of effect/log-likelihood score pairings, are then used during de novo prediction of TFBSs.

$$LLS_{\text{eQTL magnitude}} = \sum_{i=0}^N -\log_2 P(x \geq m_i | \text{human genome}) \quad (6)$$

Where  $N$  is the number of eQTLs overlapping the current putative TFBS;  $m_i$  is the magnitude of effect of an eQTL overlapping the current putative TFBS; and  $D_{\text{human genome}}$  is the distribution of all eQTL magnitudes in each nucleotide position in the human genome.

### CpG islands

Because the methylation of DNA acts as a repressor of transcription, active promoters tend to be unmethylated. When methylated, the cytosine in a CpG dinucleotide can deaminate to thymine. Therefore, a CpG ratio close to what would be expected by chance is often indicative of an active promoter region [56,57]. Subsequently, CpG ratios (observed/expected) across a 200 nucleotide (nt) window were computed for each nucleotide position in the target

genome. A distribution of these ratios was generated and used to generate log-likelihood scores for each possible ratio (Eq. 7). CpG ratio/log-likelihood score pairings are then used during de novo prediction of TFBSs.

$$LLS_{CpG} = -\log_2 P(x \geq r_{obs/exp} \text{target genome}) \quad (7)$$

Where  $r_{obs/exp}$  is the ratio of observed to expected CpG dinucleotides in a 200 bp window centered on the current putative TFBS and where  $D_{genome}$  is the distribution of  $r_{obs/exp}$  across all nucleotide locations in the target genome.

### Conservation of vertebrate DNA

Conservation of sequence analysis has been performed by Ensembl to identify constrained elements for each species in each species group via the genomic evolutionary rate profiling (GERP) tool [58]. For each of the vertebrate species of Ensembl release 94, we calculated the distance from all nucleotides in the associated species genome to the nearest GERP constrained element and generated distributions of distances that were used to calculate log-likelihood scores for each distance (Eq. 8). GERP element distance/log-likelihood score pairings for each species are then used during de novo prediction of TFBSs in the relevant species.

$$LLS_{conservation} = -\log_2 P(x \leq d_i | \text{target genome}) \quad (8)$$

Where  $d_i$  is the distance between the current putative TFBS and the nearest conserved element in an alignment of 70 mammalian genomes (GERP) and  $D_{genome}$  is the distribution of distances between all nucleotides in the target genome and the nearest GERP conserved element.

### Combined affinity score

The addition of likelihood values is an established mathematical approach for measuring the combined effect of several independent parameters [59,60]. A summation of the weight (log-likelihood) scores from each experimental dataset is then performed for each putative TFBS and is

represented as the “combined affinity score”. For analysis of human sequences, this is represented by Eq. 9. Owing to the limitations of available experimental data for nonhuman species, currently, for nonhuman vertebrates, the combined affinity score is described by Eq. 10. Complete scoring of ~80,000+ transcript promoter regions (1,000 bp) was used to generate  $p$  values for combined affinity scoring; computation was performed via the supercomputing resources of the CSC – IT Center for Science Ltd.

$$\begin{aligned} \text{Combined Affinity}_{human} \\ = Eq_1 + Eq_2 + Eq_3 + Eq_4 + Eq_5 + Eq_6 \\ + Eq_7 + Eq_8 \end{aligned} \quad (9)$$

$$\begin{aligned} \text{Combined Affinity}_{non-human} \\ = Eq_1 + Eq_2 + Eq_7 + Eq_8 \end{aligned} \quad (10)$$

### Benchmarking of several TFBS prediction tools

For comparison, in addition to TFBSFootprinter, several other TFBS prediction tools/models were used in benchmarking: the traditional PWM, DeepBind (v. 011; SELEX and ChIP-Seq models) [61], DeepSEA [62], and FIMO (meme v. 5.5.1; JASPAR 2018 nonredundant models) [63]. DeepBind was taken as an example utilizing a modern deep learning algorithm, and FIMO was chosen because it outperformed all other methods in a previous benchmark of de novo TFBS prediction tools [16]. For DeepBind, all parameters were set as defaults, analyses were performed with TF motifs on the basis of both SELEX and ChIP-Seq (when available), and the better of the two scores was retained. For DeepSEA, all parameters were set as defaults, analyses were performed with all 21,907 models, and then scores for all models matching the target TF were extracted and the best score kept. For TFBSFootprinter and FIMO, the  $p$  value threshold was set to 1, and all other settings were run as defaults. The TFBSFootprinter, FIMO, and PWM approaches all use JASPAR 2018 nonredundant TF motifs as the basis for scoring. For all the models, the top de novo prediction score for a target region (true positive or true negative) was kept as representative. For each TF, the correlating true positive and true negative scores were used to generate receiver

operating characteristic (ROC) curves and quantify the area underneath (AUROC) via the “roc\_curve” module of the scikit-learn Python library [64], which is a common method for evaluating TFBS prediction [61,65–67].

### **Benchmarking on experimentally verified TFBSs**

Experimentally verified and curated TFBSs belonging to the annotated regulatory binding sites (ABS) [68], ORegAnno [69], and Pleiades promoter project [70] databases were retrieved as GFF files from the Pazar database [71]. From these data, 504 experimentally validated binding sites affecting gene expression for 20 DeepBind TFs and 607 experimentally validated binding sites affecting gene expression for 25 JASPAR 2018 nonredundant TFs were selected. TFs were included only if they had at least 10 unique, experimentally validated TFBSs linked to gene expression changes, resulting in a final list of 14 TFs which could be compared across all prediction methods.

All target sites were converted from Hg19 to GRCh38 genomic coordinates via Ensembl REST. Subsequently, 50 bp sequences centered on each experimentally validated functional binding site in the human genome were retrieved to serve as true positives. The window length of 50 bp was chosen because it is wide enough to contain the longest TF motif (21 positions), which may overlap with the experimentally validated location at either end while also permitting some inaccuracy as to the exact center of the verified TFBS.

For each true positive, 50 true negatives were generated. True negatives were drawn at random locations within the promoter of the same Ensembl transcript of the corresponding true positive, within a 2,000 bp window (upstream and downstream) centered on each true positive, and at least 25 bp away.

### **Analyzing the effect of multiomic transcription-relevant data on TFBS prediction**

In addition to TFBSFootprinter benchmark scoring using all multiomic features, all 128 possible combinations of transcription-relevant features (PWM, CAGE, eQTL, metaclusters, ATAC-Seq, CpG, sequence conservation, expression

correlation), which include PWM as one of the components, were used in scoring the true positives and true negatives. This allowed the identification of the best possible feature-combination TFBSFootprinter model for each TF, labeled “TFBSFootprinter best by TF”, as well as the TFBSFootprinter model, which performed best on average across all TFs, labeled “TFBSFootprinter best overall”. In the assessment of the DeepBind tool, both available models, which are based on SELEX or ChIP-Seq data, were used. Using a paired-sample t test, comparisons of ROC scores were made between all of the models: TFBSFootprinter, PWM, DeepBind, DeepSEA, and FIMO.

### **Benchmarking on non-human species – mouse and zebrafish**

Unlike in humans, extensive experimentally verified and curated TFBSs are not commonly available for the great majority of the 316 non-human species which the TFBSFootprinter tool can be used to analyze. As a result, benchmarking was performed using ChIP-Seq peaks for representative model organisms of mouse (*Mus musculus*) and zebrafish (*Danio rerio*). ChIP-Seq data for 225 TFs was retrieved from the ChIP-Atlas [72] database for mouse (genome assembly GRCm38/mm10). These GRCm38 genome assembly peak coordinates were translated to GRCm39 genome assembly coordinates using Lifter [73]. ChIP-Seq data for 10 TFs was retrieved from the GTRD database [45] for zebrafish (genome assembly GRCz11). For both mouse and zebrafish analyses, for each TF we mapped each of up to the top 500 ChIP-Seq peaks (a minimum threshold of 100 peaks was set) for that TF to their nearest transcript in the target genome and used the TFBSFootprinter tool to scan a region of 200 bp centered on the center of the ChIP-Seq peak (ChIP-Seq peaks ranged in width from several 10s to 100s of base pairs). These results served as true positives. For each true positive we derived a matching true negative in the following manner: take the same TSS relative coordinates of the true positive (total of 200 bp window) but apply them to another random transcript ID in the genome of the target species which has not had a ChIP-Seq

peak for the current TF matched to it, and likewise analyze this region with TFBSFootprinter. In this way the 200 bp region analyzed is the same distance from the TSS and thus, presumably, is equivalent in potential binding/functionality. For each TF, the correlating true positive and true negative scores were used to generate ROC curves and quantify the AUROC via the “roc\_curve” module of the scikit-learn Python library [64].

## Results

### *Experimental datasets used in TFBS identification*

An outline of the TFBSFootprinter methodology is given in [Figure 1](#), including the results of an example analysis of the DNA damage repair gene BRCA2 (Breast CAncer gene 2) Ensembl transcript ENST00000380152. Importantly, the results of this example prediction match previously experimentally verified TFBSs in the BRCA2 promoter, specifically sites for USF1, ELF1, and E2F family factors [74]. Several of the other predictions are for proteins that have a known role in both DNA damage, NPAS2 [75] and ID2 [76], and breast cancer [76,77].

Experimental data from a total of six databases were incorporated into the TFBSFootprinter algorithm for analysis of human genes ([Figure 1\(a\)](#)). Data from the relevant datasets were preprocessed to generate score distributions with which putative TFBS predictions could later be compared, as described in the Methods. Each dataset allows for scoring of transcription-relevant markers in or near putative regulatory elements identified by PWM analysis: colocalization with ChIP-Seq metaclusters; cap analysis of gene expression (CAGE) peaks, ATAC-Seq peaks, or CpG islands; correlation of expression between predicted TFs and genes of interest; colocalization of eQTLs and effects on the expression of target genes; and measurement of conservation in related vertebrate species ([Figure 1\(c\)](#)). For nonhuman vertebrates, analyses are performed on the basis of preprocessed data for PWM, CpG, and conservation. The simplicity of this piecewise approach allows for easy inclusion of additional TFBS-relevant data in the future.

### *TFBSFootprinter availability*

The TFBSFootprinter tool ([https://github.com/thirtysix/TFBS\\_footprinting3](https://github.com/thirtysix/TFBS_footprinting3)) is available for installation via Conda (<https://anaconda.org/thirtysix/tfbs-footprinting3>) and as a Python library (<https://pypi.org/project/TFBS-footprinting3/>) and can subsequently be easily installed on a Linux system via the single command “pip install TFBS-footprinting3”. Owing to size considerations, supporting experimental data for both human and nonhuman species are downloaded on demand on first usage. Documentation on background, usage, and options is available both within the program and more extensively online ([tfbs-footprinting.readthedocs.io](https://tfbs-footprinting.readthedocs.io)). A listing and description of the analysis command line parameters are given in [Table 2](#).

### *The inclusion of empirical datasets improves TFBS prediction accuracy*

The performance of both individual datasets and combinations of datasets in the identification of experimentally verified functional TFBSs was tested via ROC analysis ([Figure 2](#), [Table 3](#)). Across the 14 TFs tested with all methods, the average AUROC were TFBSFootprinter with all features (0.881), TFBSFootprinter overall best (0.910), TFBSFootprinter best by TF (0.919); for the other models the values were DeepBind best by TF (0.798), DeepSEA best by TF (0.682), FIMO (0.817), and PWM (0.854). The ROC curves for TFBSFootprinter overall best and best by TF are included as [Supplementary Figure S1](#).

The TFBSFootprinter model with the best average area under the ROC curve (AUROC) across all the tested TFs was the combination of PWM, ATAC, CAGE, conservation, and metacluster data (TFBSFootprinter overall best); with an average AUROC of 0.910. A paired-sample t test revealed that this model was significantly better than PWM ( $p$  value,  $9.28 \times 10^{-3}$ ), DeepBind ( $p$  value =  $4.91 \times 10^{-3}$ ), DeepSEA ( $p$  value,  $1.79 \times 10^{-4}$ ), and FIMO ( $p$  value,  $3.75 \times 10^{-2}$ ) ([Figure 2\(b\)](#)). When all the transcription-relevant features were used, TFBSFootprinter outperformed DeepBind ( $p$  value =  $3.29 \times 10^{-2}$ ).

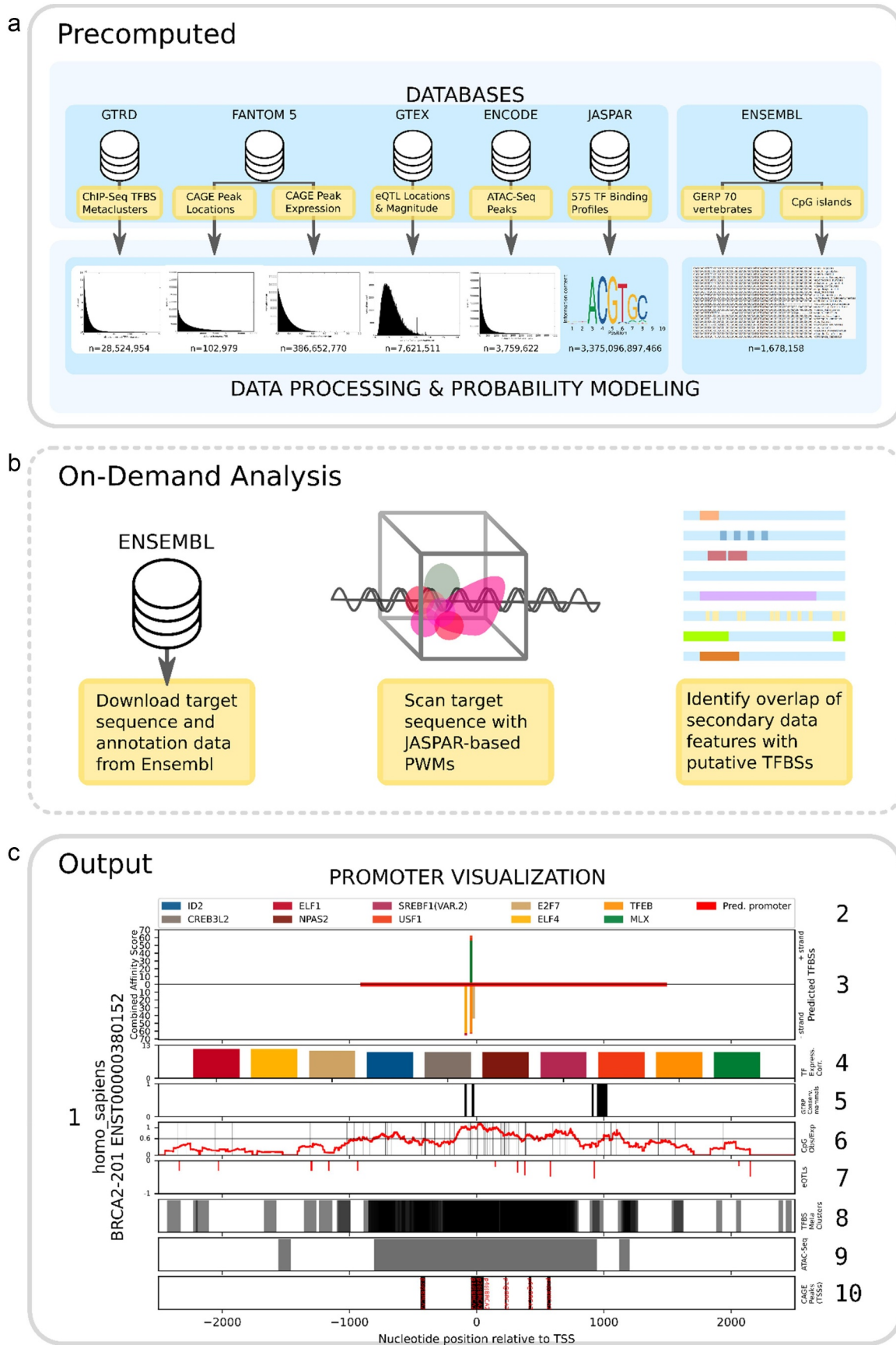


**Figure 1.** Outline of the datasets used in TFBSFootprinter. (a) A total of six empirical datasets are used to support the computational prediction of TFBSs via the TFBSFootprinter tool. The experimental data have been preprocessed to generate score distributions from which probability scores can be applied to putative TFBSs ( $n$  values indicate the number of elements used to compute distributions). (b) The user defines a target ensembl transcript ID and TSS-related start/end sites, which are then used to download the corresponding DNA sequence and annotation data via the ensembl API. PWM analysis of the DNA sequence generates putative TFBS hits, which are then compared with elements from the experimental datasets and scored via pregenerated log-likelihood scores relevant for the target genome. (c) The outputs of

**Table 2.** TFBSFootprinter parameters.

Parameter	Values	Description
-t_ids_file, -t	[Full path to filename]	Required for running an analysis. Location of a file containing Ensembl target_species transcript ids. Input options are either a text file of Ensembl transcript ids or a.csv file with individual values set for each parameter.
-tf_ids_file, -tfs	[Full path to filename]	Optional: Location of a file containing a limited list of Jaspar TFs to use in scoring DNA sequence [default: all Jaspar TFs].
-promoter_before_tss, -pb	0–100,000; default, 900	Number (integer) of nucleotides upstream of TSS to include in analysis. If this number is negative the start point will be downstream of the TSS, the end point will then need to be further downstream.
-promoter_after_tss, -pa	0–100,000; default, 100	Number (integer) of nucleotides downstream of TSS to include in analysis. If this number is negative the end point will be upstream of the TSS. The start point will then need to be further upstream.
-top_x_tfs, -tx	1–20; default, 10	Number (integer) of unique TFs to include in output.svg figure.
-pval, -p	0.0000001–1; default 0.01	P value (float) for PWM score cutoff.
-pvalc, -pc	0.0000001–1; default 0.01	P value (float) for combined affinity score score cutoff.
-exp_data_update, -update		Download the latest experimental data files for use in analysis. Will run automatically if the "data" directory does not already exist (e.g., first usage).
-nofig, -no		Do not output a figure.

### **TFBSFootprinter produces strong predictions in mouse and zebrafish**

ROC analysis of ChIP-Seq peaks was performed with TFBSFootprinter for 225 TFs in mouse and 10 TFs in zebrafish. In mouse, we observed a mean ROC AUC score of 0.777, with the lowest scoring 6 TFs (PROX1, SOX11, FOXC2, SOX4, PAX7, and TCF4) falling in a range of 0.451 to 0.498 and thus considered uninformative in prediction. A further 12 fell in the range of 0.506 to 0.598, and the remaining 207 scored a ROC AUC greater than 0.601, the full results are presented as Supplementary Table 1. Significantly fewer ChIP-Seq experiments were available for zebrafish, with the 10 TFs scoring ROC AUC values ranging from 0.506 (FOXD3) to 0.950 (CTCF), and an overall mean value of 0.715, the full results are presented as Supplementary Table 2.

### **Discussion**

We have tested the newest version [4,3,5,6] of our method for the prediction of TFBSs and introduce a tool that allows analyses of promoters in 317 vertebrate species, with automatic sequence retrieval and analysis on the basis of the Ensembl transcript ID. The method leverages transcription-relevant data to augment the prediction of functional TFBSs beyond the classical PWM. In benchmarking, the TFBSFootprinter method scored evenly or better than the traditional PWM, DeepBind, DeepSEA, and FIMO models when all the transcription-relevant data were used in its scoring. Surprisingly, benchmarking revealed that several types of transcription-relevant data, specifically eQTLs and gene expression correlations between putative TFs and target genes, did not contribute significantly to the prediction of TFBSs. As a result, the combination of

the TFBSFootprinter analysis are a table of results, including predicted TFBS names, locations, and scoring for each metric (not pictured), as well as individual files containing sequences and annotations. A publication-ready scalable vector graphics file (.Svg) is also produced, containing several elements as indicated and described. (C1) HUGO gene nomenclature committee (HGNC)-based identifier + ensembl transcript ID. (C2) color-coded legend of the top 10 TFs predicted to bind to this promoter. (C3) graphical representation of the promoter of the transcript where the predicted binding sites are indicated by colored bars. The bar height indicates the combined affinity score, and the bars on the positive y-axis indicate binding on the positive (sense) strand, and the negative y-axis represents the negative (antisense) strand. (C4) log-likelihood score of the correlation of expression between each top predicted TF gene and the target gene. (C5) highly conserved regions of 70-mammal alignment as determined by GERP analysis (black bars). (C6) vertical lines represent CpG locations. The red line indicates the CpG ratio of the promoter sequence over a 200 bp window. (C7) genetic variants identified in the GTEx database that affect target gene expression (eQTLs). Green indicates a positive impact on expression (positive y-axis), and red indicates a negative impact (negative y-axis). (C8) TFBS metaclusters identified in the GTRD database (gray bars). (C9) ATAC-seq peaks (open chromatin) across many different cell types retrieved from the ENCODE database (gray bars). (C10) CAGE peaks indicating TSSs identified in the FANTOM database (black bars). The nucleotide positions at the bottom are relative to the ensembl-defined transcription start site of the target transcript and apply to C3 and C5–C10.

**Table 3.** AUROC results of the TFBS prediction method.

TF	TFBSFootprinter best by TF	TFBSFootprinter overall best	TFBSFootprinter all features	DeepBind best by TF	DeepSEA	FIMO	PWM
SRF	0.910	0.869	0.802	0.950	0.522	0.982	0.896
FOXA2	0.972	0.971	0.955	0.615	0.657	0.585	0.763
SPI1	0.967	0.967	0.939	0.905	0.835	0.911	0.941
TBP	0.967	0.942	0.876	0.662	0.302	0.959	0.946
E2F1	0.960	0.940	0.883	0.854	0.576	0.922	0.923
FOXA1	0.908	0.908	0.887	0.948	0.877	0.952	0.869
JUN	0.941	0.939	0.889	0.876	0.735	0.789	0.899
FOS	0.938	0.938	0.921	0.785	0.890	0.840	0.865
HNF1A	0.916	0.899	0.875	0.835	0.791	0.908	0.883
TFAP2A	0.914	0.914	0.887	0.752	0.657	0.724	0.828
HNF4A	0.905	0.904	0.896	0.907	0.841	0.879	0.854
REST	0.894	0.889	0.874	0.722	0.759	0.771	0.857
SP1	0.852	0.851	0.838	0.804	0.515	0.810	0.821
GATA3	0.825	0.810	0.810	0.562	0.588	0.405	0.608

features that produced the highest average ROC score across all tested TFs was PWM, ATAC, CAGE, conservation, and metaclusters. In paired-sample t test analysis, the TFBSFootprinter model performs significantly better than all the other models do. In addition, we identified specific combinations of transcription-relevant data that produced the best ROC scores for each tested TF; these combinations may lead to customizing TF models in the future. The low performance of the features related to RNA expression may be the result of the use of data that are not tissue specific; this is grounds for further research, as TFs, like many other proteins, can have tissue-specific expression patterns.

The results of testing TFBSFootprinter on ChIP-Seq peaks in mouse and zebrafish were promising. In mouse we observed that 207 of 225 tested TFs had ROC AUC scores greater than 0.60, and likewise in zebrafish the result was 8 of 10 tested TFs. As with experimentally validated TFBSs, ChIP-Seq data itself is at best sparse outside of the most researched species, and completely absent in the vast majority of others. The GEO database contains ChIP-Seq experiments with BED file data for just 16 vertebrate species, which quickly tapers off in experiment count: after 18,771 experiments for *Homo sapiens* and 6,864 for *Mus musculus* there is a more than 100-fold drop-off for the next most common species, *Rattus norvegicus* with 66 experiments. While we may only infer that TFBSFootprinter prediction of functional TFBSs matches the performance we observed in humans, as it incorporates four of the five top-performing transcription-relevant

data (Figure 2), we do have direct evidence from our analyses in mouse and zebrafish that ChIP-Seq peaks scores are well reproduced by the tool.

We believe that TFBSFootprinter provides an excellent way to predict TFBSs as a high-performing model overall but also because of the ease of use in working with many vertebrate organisms. TFBSFootprinter may therefore supplement current investigations into gene function or provide a means to perform larger-scale analyses of groups of related target genes. After analysis of a target transcript, a publication-ready figure depicting the top scoring TFBS candidates is produced. Additionally, a number of tables (.csv) and JavaScript Object Notation (.json) files presenting various aspects of the results are output. Primary among these is a list of computational predictions in the target species that are supported by empirical data, which are sorted by a sum of the combined log likelihood scores (the combined affinity score). Importantly, scoring of nonhuman species is limited by the availability of external data for that species; at this time, the only data commonly available for nonhuman species are proximity to transcription hotspots (CAGE-like peaks), sequence conservation, CpG, and JASPAR motif data. Updates of species which are available for analysis are ongoing.

### TFBSFootprinter availability

The TFBSFootprinter tool is available as a Python package and can be installed via PyPi or Conda. Any Ensembl transcript ID from any of 317

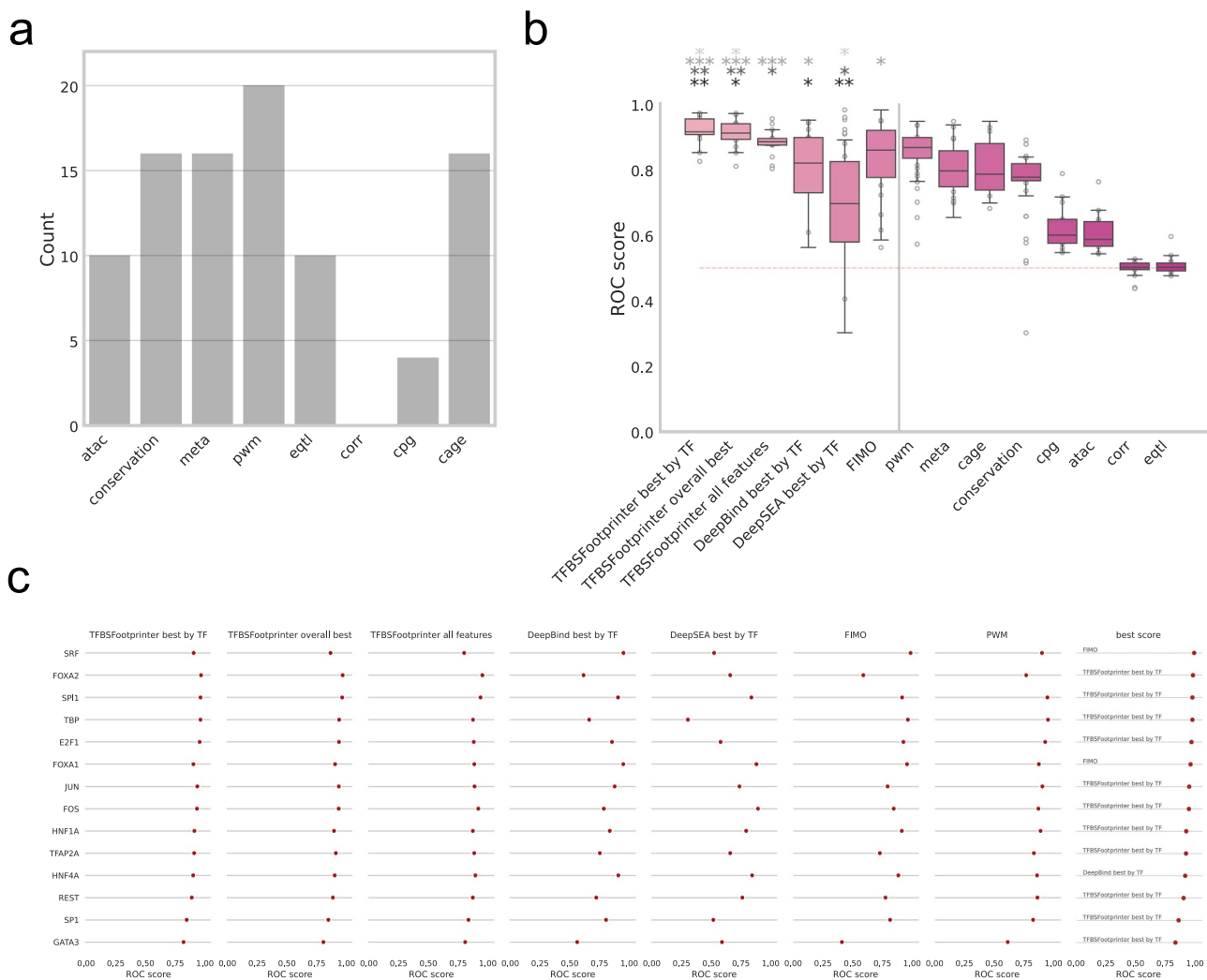


**Figure 2.** ROC analysis model performance in the identification of experimentally verified functional TFBSs—random locations in the same Ensembl transcript. ROC analysis was performed via experimentally verified functional TFBSs as annotated in the ORegAnno/Pleiades/ABS datasets as true positives, where true negatives were random locations in other Ensembl transcripts at the same distance from the TSS as the associated true positive. All the ROC curve analyses were performed on the TFs that had at least 10 true positives and at least 50 true negatives per true positive were used for each analysis. Each true positive/negative segment analyzed was 50 nucleotides long, and the highest TFBS score for the relevant dataset(s) was used for each true positive/negative segment. (a) bar plot of the frequency of experimental data types in the top 20 performing TFBSFootprinter models. (b) boxplot of ROC scores for TFBSFootprinter, DeepBind, DeepSEA, and FIMO for 14 TFs (left of vertical bar). ROC scores were also calculated using individual experimental metrics to show how well each contributes to accuracy of the combined model (right of vertical bar). (c) ROC scores for each individual TF tested for each primary TFBS prediction model under study. The best scoring model among all the models is named for each TF (right). TFBSFootprinter best by TF, which is based on using the highest ROC score achieved by some combination of experimental data models; TFBSFootprinter overall best, based on using the combination of experimental data models that had the best average ROC score across all the TFs analyzed; DeepBind best by TF, which is based on using the higher ROC score of the SELEX or CHIP-Seq DeepBind models. Black asterisks (bottom row) denote significant difference of first six models with ‘pwm’ model; dark gray asterisks (second from bottom row) denote significant difference between first six models and ‘DeepBind’ model; light gray asterisks (second from top row) denote significant difference between first six models and ‘DeepSEA’ model; silver asterisks (top row) denote significant difference between first six models and ‘FIMO’ model; as determined by related t-test.

\*p-value < 0.05, \*\*p-value < 0.005, and \*\*\*p-value < 0.0005

vertebrate species available in the Ensembl database can be used as input. Starting with a list of Ensembl transcript ids for a target species (e.g., Homo sapiens), TFBSFootprinter will download

a user-defined region of DNA sequence from the Ensembl server. The sequence is then scored using up to 575 JASPAR TFBS profiles or a more limited set as defined by the user. Each putative TFBS is

then additionally scored on the basis of transcription-relevant data, which may include, depending on the target species, proximity/overlap with the TSS, TFBS metaclusters, open chromatin, eQTLs that affect expression levels of the proximal gene, conservation of sequence, correlation of expression with the proximal (target) gene, and CpG content.

### Limitations

In the benchmark, true negatives were defined on the basis of random locations that did not overlap with experimentally verified true positives. However, there is no guarantee that these sites are indeed devoid of any binding/functionality for the TFs in question. This is a notable problem in the testing of TFBS prediction, with random sites being one of the best solutions, although it is imperfect [66]. Not all vertebrate TF binding models cataloged in the JASPAR database are applicable to every vertebrate species, as not all species possess the same genes. Users will be required to ensure that any predicted TF has an ortholog in any species in which they perform TFBS prediction.

Two of the benchmarks were scored on ChIP-Seq data from the GTRD database, and because GTRD metaclusters are part of the TFBSFootprinter scoring model, some bias is introduced. However, metaclusters are defined by merging all ChIP-Seq data (all TFs, therefore TF agnostic) across all peak-calling methods (four separate peak-calling methods), and benchmarking was performed on ChIP-Seq data from one peak-calling method for individual TFs. We chose to perform TFBSFootprinter analysis using all the available transcription-relevant features. In the future, we plan to expand the testing and assessment of empirical datasets and incorporate an option to use the combination of features that is proven best for each individual TF.

TFBSFootprinter integrates multiple transcription-relevant features (e.g., conservation, ChIP-Seq metaclusters, CpG content, and TSS proximity) to support prediction of TFBSs; the tool is not intended for independent analysis of these features outside of their role in TFBS prediction.

### Acknowledgments

Heini Huhtala is acknowledged for assistance in statistical techniques and professor Matti Nykter and Payam Emami Khoonsari PhD are gratefully thanked for discussions on practical and theoretical concerns. The non-profit CSC – IT Center for Science Ltd, owned by the state of Finland and Finnish higher education institutions, is acknowledged for providing computational resources for analyses.

### Disclosure statement

No potential conflict of interest was reported by the author(s).

### Funding

This work was supported by the Finnish Cultural Foundation and Fimlab to HB, and Academy of Finland and Jane & Aatos Erkko Foundation to SP.

### Data availability statement

The TFBSFootprinter project page is located at [https://github.com/thirtysix/TFBS\\_footprinting3](https://github.com/thirtysix/TFBS_footprinting3). Results of benchmarking of TFBSFootprinter (<https://osf.io/hzny6/>) are available as Open Science Foundation repositories.

### Abbreviations

ATAC-Seq	Assay for transposase-accessible chromatin by sequencing
bp	Base pairs
CAGE)	Cap analysis of gene expression
ChIP-Seq	Chromatin immunoprecipitation with massively parallel DNA sequencing
CRE)	Cis-regulatory element
eQTL	Expression quantitative trait locus
HT-SELEX	High-throughput systematic evolution of ligands by exponential enrichment
PFM	Position frequency matrix
PWM	Position weight matrix
TF	Transcription factor
TFBS	Transcription factor binding site
TSS	Transcription start site

### ORCID

Harlan R. Barker  <http://orcid.org/0000-0003-4125-2522>

### References

- [1] Lambert SA, Jolma A, Campitelli LF, et al. The human transcription factors. *Cell*. 2018;172(4):650–665. doi: 10.1016/j.cell.2018.01.029

- [2] Wittkopp PJ, Kalay G. Cis-regulatory elements: molecular mechanisms and evolutionary processes underlying divergence. *Nat Rev Genet.* 2011;13(1):59–69. doi: [10.1038/nrg3095](https://doi.org/10.1038/nrg3095)
- [3] Barker H, Aaltonen M, Pan P, et al. Role of carbonic anhydrases in skin wound healing. *Exp Mol Med.* 2017;49(5):e334–e334. doi: [10.1038/emm.2017.60](https://doi.org/10.1038/emm.2017.60)
- [4] Karjalainen SL, Haapasalo HK, Aspatwar A, et al. Carbonic anhydrase related protein expression in astrocytomas and oligodendroglial tumors. *BMC Cancer.* 2018;18(1):584. doi: [10.1186/s12885-018-4493-4](https://doi.org/10.1186/s12885-018-4493-4)
- [5] Barker H, Parkkila S, Bader M. Bioinformatic characterization of angiotensin-converting enzyme 2, the entry receptor for SARS-CoV-2. *PLOS ONE.* 2020;15(10):e0240647. doi: [10.1371/journal.pone.0240647](https://doi.org/10.1371/journal.pone.0240647)
- [6] Arppo A, Barker H, Parkkila S, et al. Bioinformatic characterization of ENPEP, the gene encoding a potential cofactor for SARS-CoV-2 infection. *PLOS ONE.* 2024;19(12):e0307731. doi: [10.1371/journal.pone.0307731](https://doi.org/10.1371/journal.pone.0307731)
- [7] Chiu TP, Rao S, Mann RS, et al. Genome-wide prediction of minor-groove electrostatic potential enables biophysical modeling of protein-DNA binding. *Nucleic Acids Res.* 2017;45(21):12565–12576. doi: [10.1093/nar/gkx915](https://doi.org/10.1093/nar/gkx915)
- [8] Rohs R, Jin X, West SM, et al. Origins of specificity in protein-DNA recognition. *Annu Rev Biochem.* 2010;79(1):233–269. doi: [10.1146/annurev-biochem-060408-091030](https://doi.org/10.1146/annurev-biochem-060408-091030)
- [9] Zhou T, Yang L, Lu Y, et al. Dnashape: a method for the high-throughput prediction of DNA structural features on a genomic scale. *Nucleic Acids Res.* 2013;41(W1):W56–62. doi: [10.1093/nar/gkt437](https://doi.org/10.1093/nar/gkt437)
- [10] Chiu TP, Yang L, Zhou T, et al. Gbshape: a genome browser database for DNA shape annotations. *Nucleic Acids Res.* 2015;43(D1):D103–9. doi: [10.1093/nar/gku977](https://doi.org/10.1093/nar/gku977)
- [11] Zhou T, Shen N, Yang L, et al. Quantitative modeling of transcription factor binding specificities using DNA shape. *Proc Natl Acad Sci U S A.* 2015;112(15):4654–4659. doi: [10.1073/pnas.1422023112](https://doi.org/10.1073/pnas.1422023112)
- [12] Pique-Regi R, Degner JF, Pai AA, et al. Accurate inference of transcription factor binding from DNA sequence and chromatin accessibility data. *Genome Res.* 2011;21(3):447–455. doi: [10.1101/gr.112623.110](https://doi.org/10.1101/gr.112623.110)
- [13] Sherwood RI, Hashimoto T, O'Donnell CW, et al. Discovery of directional and nondirectional pioneer transcription factors by modeling DNase profile magnitude and shape. *Nat Biotechnol.* 2014;32(2):171–178. doi: [10.1038/nbt.2798](https://doi.org/10.1038/nbt.2798)
- [14] Deplancke B, Alpern D, Gardeux V. The genetics of transcription factor DNA binding variation. *Cell.* 2016;166(3):538–554. doi: [10.1016/j.cell.2016.07.012](https://doi.org/10.1016/j.cell.2016.07.012)
- [15] Qian Z, Lu L, Liu X, et al. An approach to predict transcription factor DNA binding site specificity based upon gene and transcription factor functional categorization. *Bioinformatics.* 2007;23(18):2449–2454. doi: [10.1093/bioinformatics/btm348](https://doi.org/10.1093/bioinformatics/btm348)
- [16] Khamis AM, Motwalli O, Oliva R, et al. A novel method for improved accuracy of transcription factor binding site prediction. *Nucleic Acids Res.* 2018;46(12):e72. doi: [10.1093/nar/gky237](https://doi.org/10.1093/nar/gky237)
- [17] Duren Z, Chen X, Jiang R, et al. Modeling gene regulation from paired expression and chromatin accessibility data. *Proc Natl Acad Sci U S A.* 2017;114(25):E4914–E4923. doi: [10.1073/pnas.1704553114](https://doi.org/10.1073/pnas.1704553114)
- [18] Li Z, Schulz MH, Look T, et al. Identification of transcription factor binding sites using ATAC-seq. *Genome Biol.* 2019;20(1):45. doi: [10.1186/s13059-019-1642-2](https://doi.org/10.1186/s13059-019-1642-2)
- [19] Ruan S, Stormo GD. Comparison of discriminative motif optimization using matrix and DNA shape-based models. *BMC Bioinformatics.* 2018;19(1):86. doi: [10.1186/s12859-018-2104-7](https://doi.org/10.1186/s12859-018-2104-7)
- [20] Jayaram N, Usvyat D, Martin ACR. Evaluating tools for transcription factor binding site prediction. *BMC Bioinformatics.* 2016;17(1):547. doi: [10.1186/s12859-016-1298-9](https://doi.org/10.1186/s12859-016-1298-9)
- [21] Heinz S, Benner C, Spann N, et al. Simple combinations of lineage-determining transcription factors prime cis-regulatory elements required for macrophage and B cell identities. *Mol Cell.* 2010;38(4):576–589. doi: [10.1016/j.molcel.2010.05.004](https://doi.org/10.1016/j.molcel.2010.05.004)
- [22] Reid JE, Wernisch L. STEME: efficient EM to find motifs in large data sets. *Nucleic Acids Res.* 2011;39(18):e126. doi: [10.1093/nar/gkr574](https://doi.org/10.1093/nar/gkr574)
- [23] Li Y, Ni P, Zhang S, et al. ProSampler: an ultrafast and accurate motif finder in large ChIP-seq datasets for combinatorial motif discovery. *Bioinformatics.* 2019;35(22):4632–4639. doi: [10.1093/bioinformatics/btz290](https://doi.org/10.1093/bioinformatics/btz290)
- [24] Bailey TL, Birol I. STREME: accurate and versatile sequence motif discovery. *Bioinformatics.* 2021;37(18):2834–2840. doi: [10.1093/bioinformatics/btab203](https://doi.org/10.1093/bioinformatics/btab203)
- [25] Tognon M, Giugno R, Pinello L. A survey on algorithms to characterize transcription factor binding sites. *Brief Bioinform.* 2023;24(3). doi: [10.1093/bib/bbad156](https://doi.org/10.1093/bib/bbad156)
- [26] Vlieghe D, Sandelin A, De Bleser PJ, et al. A new generation of JASPAR, the open-access repository for transcription factor binding site profiles. *Nucleic Acids Res.* 2006;34(Database issue):D95–7. doi: [10.1093/nar/gkj115](https://doi.org/10.1093/nar/gkj115)
- [27] Castro-Mondragon JA. JASPAR 2022: the 9th release of the open-access database of transcription factor binding profiles. *Nucleic Acids Res.* 2022;50(D1):D165–D173. doi: [10.1093/nar/gkab1113](https://doi.org/10.1093/nar/gkab1113)
- [28] Wingender E, Dietze P, Karas H, et al. TRANSFAC: a database on transcription factors and their DNA binding sites. *Nucleic Acids Res.* 1996;24(1):238–41. doi: [10.1093/nar/24.1.238](https://doi.org/10.1093/nar/24.1.238)
- [29] Berman BP, Nibu Y, Pfeiffer BD, et al. Exploiting transcription factor binding site clustering to identify cis-regulatory modules involved in pattern formation

- in the drosophila genome. *Proc Natl Acad Sci U S A*. 2002;99(2):757–762. doi: [10.1073/pnas.231608898](https://doi.org/10.1073/pnas.231608898)
- [30] Cusanovich DA, Pavlovic B, Pritchard JK, et al. The functional consequences of variation in transcription factor binding. *PLoS Genet*. 2014;10(3):e1004226. doi: [10.1371/journal.pgen.1004226](https://doi.org/10.1371/journal.pgen.1004226)
- [31] Hemberg M, Kreiman G. Conservation of transcription factor binding events predicts gene expression across species. *Nucleic Acids Res*. 2011;39(16):7092–7102. doi: [10.1093/nar/gkr404](https://doi.org/10.1093/nar/gkr404)
- [32] Wenger AM, Clarke SL, Guturu H, et al. PRISM offers a comprehensive genomic approach to transcription factor function prediction. *Genome Res*. 2013;23(5):889–904. doi: [10.1101/gr.139071.112](https://doi.org/10.1101/gr.139071.112)
- [33] Koudritsky M, Domany E. Positional distribution of human transcription factor binding sites. *Nucleic Acids Res*. 2008;36(21):6795–6805. doi: [10.1093/nar/gkn752](https://doi.org/10.1093/nar/gkn752)
- [34] Haynes BC, Maier EJ, Kramer MH, et al. Mapping functional transcription factor networks from gene expression data. *Genome Res*. 2013;23(8):1319–1328. doi: [10.1101/gr.150904.112](https://doi.org/10.1101/gr.150904.112)
- [35] Ma S, Snyder M, Dinesh-Kumar SP. Discovery of novel human gene regulatory modules from gene Co-expression and promoter Motif Analysis. *Sci Rep*. 2017;7(1):5557. doi: [10.1038/s41598-017-05705-2](https://doi.org/10.1038/s41598-017-05705-2)
- [36] Lonsdale J, Thomas J, Salvatore M, et al. The genotype-tissue expression (GTEx) project. *Nat Genet*. 2013;45(6):580–585. doi: [10.1038/ng.2653](https://doi.org/10.1038/ng.2653)
- [37] Chen J, Rozowsky J, Galeev TR, et al. A uniform survey of allele-specific binding and expression over 1000-genomes-project individuals. *Nat Commun*. 2016;7(1):11101. doi: [10.1038/ncomms11101](https://doi.org/10.1038/ncomms11101)
- [38] Shi W, Fornes O, Mathelier A, et al. Evaluating the impact of single nucleotide variants on transcription factor binding. *Nucleic Acids Res*. 2016;44:10106–10116. doi: [10.1093/nar/gkw691](https://doi.org/10.1093/nar/gkw691)
- [39] Maurano MT, Humbert R, Rynes E, et al. Systematic localization of common disease-associated variation in regulatory DNA. *Science*. 2012;337(6099):1190–1195. doi: [10.1126/science.1222794](https://doi.org/10.1126/science.1222794)
- [40] Davie K, Jacobs J, Atkins M, et al. Discovery of transcription factors and regulatory regions driving in vivo tumor development by ATAC-seq and FAIRE-seq open chromatin profiling. *PLoS Genet*. 2015;11(2):e1004994. doi: [10.1371/journal.pgen.1004994](https://doi.org/10.1371/journal.pgen.1004994)
- [41] Jolma A, Yan J, Whittington T, et al. DNA-binding specificities of human transcription factors. *Cell*. 2013;152(1–2):327–339. doi: [10.1016/j.cell.2012.12.009](https://doi.org/10.1016/j.cell.2012.12.009)
- [42] Wang J, Zhuang J, Iyer S, et al. Factorbook.Org: a wiki-based database for transcription factor-binding data generated by the ENCODE consortium. *Nucleic Acids Res*. 2013;41(D1):D171–6. doi: [10.1093/nar/gks1221](https://doi.org/10.1093/nar/gks1221)
- [43] Hammal F, de Langen P, Bergon A, et al. ReMap 2022: a database of human, mouse, Drosophila and Arabidopsis regulatory regions from an integrative analysis of DNA-binding sequencing experiments. *Nucleic Acids Res*. 2022;50(D1):D316–D325. doi: [10.1093/nar/gkab996](https://doi.org/10.1093/nar/gkab996)
- [44] Zheng R, Wan C, Mei S, et al. Cistrome data browser: expanded datasets and new tools for gene regulatory analysis. *Nucleic Acids Res*. 2019;47(D1):D729–D735. doi: [10.1093/nar/gky1094](https://doi.org/10.1093/nar/gky1094)
- [45] Kolmykov S, Yevshin I, Kulyashov M, et al. GTRD: an integrated view of transcription regulation. *Nucleic Acids Res*. 2021;49(D1):D104–D111. doi: [10.1093/nar/gkaa1057](https://doi.org/10.1093/nar/gkaa1057)
- [46] Fantom Consortium, the, Riken Pmi, Clst, Forrest AR, Kawaji H. A promoter-level mammalian expression atlas. *Nature*. 2014;507:462–470. doi: [10.1038/nature13182](https://doi.org/10.1038/nature13182)
- [47] Yates AD, Achuthan P, Akanni W, et al. Ensembl 2020. *Nucleic Acids Res*. 2020;48(D1):D682–D688. doi: [10.1093/nar/gkz966](https://doi.org/10.1093/nar/gkz966)
- [48] Khan A, Fornes O, Stigliani A, et al. JASPAR 2018: update of the open-access database of transcription factor binding profiles and its web framework. *Nucleic Acids Res*. 2018;46(D1):D260–D266. doi: [10.1093/nar/gkx1126](https://doi.org/10.1093/nar/gkx1126)
- [49] Nishida K, Frith MC, Nakai K. Pseudocounts for transcription factor binding sites. *Nucleic Acids Res*. 2009;37(3):939–944. doi: [10.1093/nar/gkn1019](https://doi.org/10.1093/nar/gkn1019)
- [50] Yamagishi ME, Shimabukuro AI. Nucleotide frequencies in human genome and fibonacci numbers. *Bull Math Biol*. 2008;70(3):643–653. doi: [10.1007/s11538-007-9261-6](https://doi.org/10.1007/s11538-007-9261-6)
- [51] Virtanen P, Gommers R, Oliphant TE, et al. SciPy 1.0: fundamental algorithms for scientific computing in python. *Nat Methods*. 2020;17(3):261–272. doi: [10.1038/s41592-019-0686-2](https://doi.org/10.1038/s41592-019-0686-2)
- [52] Yevshin I, Sharipov R, Valeev T, et al. GTRD: a database of transcription factor binding sites identified by ChIP-seq experiments. *Nucleic Acids Res*. 2017;45(D1):D61–D67. doi: [10.1093/nar/gkw951](https://doi.org/10.1093/nar/gkw951)
- [53] Buenrostro JD, Giresi PG, Zaba LC, et al. Transposition of native chromatin for fast and sensitive epigenomic profiling of open chromatin, DNA-binding proteins and nucleosome position. *Nat Methods*. 2013;10(12):1213–1218. doi: [10.1038/nmeth.2688](https://doi.org/10.1038/nmeth.2688)
- [54] Liu S, Zibetti C, Wan J, et al. Assessing the model transferability for prediction of transcription factor binding sites based on chromatin accessibility. *BMC Bioinformatics*. 2017;18(1):355. doi: [10.1186/s12859-017-1769-7](https://doi.org/10.1186/s12859-017-1769-7)
- [55] GTEx Consortium, Laboratory, Data Analysis & Coordinating Center (LDACC)—Analysis Working Group, Statistical Methods groups—Analysis Working Group, Enhancing GTEx (eGTEx) groups, NIH Common Fund, NIH/NCI, et al. Genetic effects on gene expression across human tissues. *Nature*. 2017;550(7675):204–213. doi: [10.1038/nature24277](https://doi.org/10.1038/nature24277)
- [56] Cohen NM, Kenigsberg E, Tanay A. Primate CpG islands are maintained by heterogeneous evolutionary

- regimes involving minimal selection. *Cell*. 2011;145(5):773–786. doi: [10.1016/j.cell.2011.04.024](https://doi.org/10.1016/j.cell.2011.04.024)
- [57] Long HK, Sims D, Heger A, et al. Epigenetic conservation at gene regulatory elements revealed by non-methylated DNA profiling in seven vertebrates. *Elife*. 2013;2:e00348. doi: [10.7554/eLife.00348](https://doi.org/10.7554/eLife.00348)
- [58] Cooper GM, Stone EA, Asimenos G, et al. Distribution and intensity of constraint in mammalian genomic sequence. *Genome Res*. 2005;15(7):901–913. doi: [10.1101/gr.3577405](https://doi.org/10.1101/gr.3577405)
- [59] Lindsay BG. Statistical inference from stochastic processes. Providence, UNITED STATES: American Mathematical Society; 1988. Available from: <http://ebookcentral.proquest.com/lib/tampere/detail.action?docID=3112866>
- [60] Fraser DAS, Reid N. Combining likelihood and significance functions. *Stat Sin*. 2020;30:1–15. Available from: <https://www.jstor.org/stable/26892772>
- [61] Alipanahi B, Delong A, Weirauch MT, et al. Predicting the sequence specificities of DNA- and RNA-binding proteins by deep learning. *Nat Biotechnol*. 2015;33(8):831–838. doi: [10.1038/nbt.3300](https://doi.org/10.1038/nbt.3300)
- [62] Chen KM, Wong AK, Troyanskaya OG, et al. A sequence-based global map of regulatory activity for deciphering human genetics. *Nat Genet*. 2022;54(7):940–949. doi: [10.1038/s41588-022-01102-2](https://doi.org/10.1038/s41588-022-01102-2)
- [63] Grant CE, Bailey TL, Noble WS. FIMO: scanning for occurrences of a given motif. *Bioinformatics*. 2011;27(7):1017–1018. doi: [10.1093/bioinformatics/btr064](https://doi.org/10.1093/bioinformatics/btr064)
- [64] Pedregosa F, Varoquaux G, Gramfort A, et al. Scikit-learn: machine learning in python. *J Mach Learn Res*. 2011;12:2825–2830. Available from: <https://www.jmlr.org/papers/v12/pedregosa11a.html>
- [65] Mathelier A, Wasserman WW, Ioshikhes I. The next generation of transcription factor binding site prediction. *PLoS Comput Biol*. 2013;9(9):e1003214. doi: [10.1371/journal.pcbi.1003214](https://doi.org/10.1371/journal.pcbi.1003214)
- [66] Sand O, Turatsinze J-V, van Helden J. Evaluating the prediction of cis-acting regulatory elements in genome sequences. In: Frishman D Valencia A, editors. *Modern genome annotation: the BioSapiens network*. Vienna: Springer Vienna; 2008. p. 55–89. doi: [10.1007/978-3-211-75123-7\\_4](https://doi.org/10.1007/978-3-211-75123-7_4)
- [67] Park S, Koh Y, Jeon H, et al. Enhancing the interpretability of transcription factor binding site prediction using attention mechanism. *Sci Rep*. 2020;10(1):13413. doi: [10.1038/s41598-020-70218-4](https://doi.org/10.1038/s41598-020-70218-4)
- [68] Blanco E, Farré D, Albà MM, et al. ABS: a database of annotated regulatory binding sites from orthologous promoters. *Nucleic Acids Res*. 2006;34(90001):D63–7. doi: [10.1093/nar/gkj116](https://doi.org/10.1093/nar/gkj116)
- [69] Lesurf R, Cotto KC, Wang G, et al. ORegAnno 3.0: a community-driven resource for curated regulatory annotation. *Nucleic Acids Res*. 2016;44(D1):D126–32. doi: [10.1093/nar/gkv1203](https://doi.org/10.1093/nar/gkv1203)
- [70] Portales-Casamar E, Swanson DJ, Liu L, et al. A regulatory toolbox of MiniPromoters to drive selective expression in the brain. *Proc Natl Acad Sci U S A*. 2010;107(38):16589–16594. doi: [10.1073/pnas.1009158107](https://doi.org/10.1073/pnas.1009158107)
- [71] Portales-Casamar E, Kirov S, Lim J, et al. PAZAR: a framework for collection and dissemination of cis-regulatory sequence annotation. *Genome Biol*. 2007;8(10):R207. doi: [10.1186/gb-2007-8-10-r207](https://doi.org/10.1186/gb-2007-8-10-r207)
- [72] Zou Z, Ohta T, Oki S. ChIP-atlas 3.0: a data-mining suite to explore chromosome architecture together with large-scale regulome data. *Nucleic Acids Res*. 2024;52(W1):W45–W53. doi: [10.1093/nar/gkae358](https://doi.org/10.1093/nar/gkae358)
- [73] Hinrichs AS, Karolchik D, Baertsch R, et al. The UCSC genome browser database: update 2006. *Nucleic Acids Res*. 2006;34(90001):D590–8. doi: [10.1093/nar/gkj144](https://doi.org/10.1093/nar/gkj144)
- [74] Davis PL, Miron A, Andersen LM, et al. Isolation and initial characterization of the BRCA2 promoter. *Oncogene*. 1999;18(44):6000–6012. doi: [10.1038/sj.onc.1202990](https://doi.org/10.1038/sj.onc.1202990)
- [75] Hoffman AE, Zheng T, Ba Y, et al. The circadian gene NPAS2, a putative tumor suppressor, is involved in DNA damage response. *Mol Cancer Res*. 2008;6(9):1461–1468. doi: [10.1158/1541-7786.MCR-07-2094](https://doi.org/10.1158/1541-7786.MCR-07-2094)
- [76] Gianni P, Matenoglou E, Geropoulos G, et al. The Fanconi anemia pathway and breast cancer: a comprehensive review of clinical data. *Clin Breast Cancer*. 2022;22(1):10–25. doi: [10.1016/j.clbc.2021.08.001](https://doi.org/10.1016/j.clbc.2021.08.001)
- [77] Zienolddiny S, Haugen A, Lie J-A, et al. Analysis of polymorphisms in the circadian-related genes and breast cancer risk in Norwegian nurses working night shifts. *Breast Cancer Res*. 2013;15(4):R53. doi: [10.1186/bcr3445](https://doi.org/10.1186/bcr3445)